厚生科学研究費補助金　（医療機器開発推進研究事業ナノメディシン研究）

分担研究報告書

ナノ分子イメージングを活用した次世代創薬アプローチ

分担研究項目　創薬標的タンパクの構造解析 - 1

分担研究者　武田　壮一　　国立循環器病センター研究所心臓生理部　室長

盛　英三　　東海大学医学部基礎医学系　教授

研究要旨：循環器疾患、脳神経疾患等の制圧のためにナノ分子イメージングを活用して新しい治療法の開発を推進することを目的とする。本分担研究では、分子の構造決定に基づく創薬を目指した研究を行う。本年度の標的タンパクとしてPKAリン酸化部位を含むヒト心筋トロポニン・コアドメインをターゲットとして新規結晶3種類の構造解析を行った。内一つの結晶系について2Å分解能の精密構造を得ることに成功し、心筋トロポニンを対象とした創薬への基盤情報を得た。

A. 研究目的

心筋の収縮は重合アクチンから成る細い繊維とモータータンパク質ミオシンから成る太い繊維それぞれの繊維間の滑りにより引き起こされる。この滑りは心筋細胞内カルシウムイオン濃度により調節され、その調節の要を司るのが、アクチン繊維上にある調節タンパク質トロポニンおよびトロポミオシンである。我々は2003年に世界に先駆けてトロポニンの活性中心であるコアドメインの結晶構造の解明に成功した(Takeda et al. Nature (2003))。この結晶構造については結晶を得るために心筋トロポニンTnIに特異的に存在するAキナーゼ（PKA）によるリン酸化部位を切除したコンストラクトを用いたため、この部位の構造情報が含まれていない。PKAリン酸化による心筋のカルシウム感受性の変調機構の分子機構を知ることは重要な生理機能の理解にとどまらず、トロポニンをターゲットにした新たなカルシウム感受性変調薬物（カルシウムセンシタイザー、カルシウムデセンシタイザーなど）をデザインする上で重要な構造情報を与えると考えられる。そこで本研究ではまずPKAリン酸化部位を含む全長ヒト心筋TnIおよびTnTとTnCから成る心筋トロポニン･コアドメインを調製、結晶化しX線結晶構造解析により構造決定を行うことを目的とする。

B. 研究方法

ヒト心筋TnT, TnIおよびTnCをそれぞれ大腸菌に大量発現し、個別に各種クロマトグラフィーにより精製した。各サブユニットを６M尿素存在下で再構成し、再構成された三量体成分を陰イオン交換カラムで単離した。単離した再構成トロポニン（Tn58K）を用いてSitting-drop法により結晶化スクリーニングを行った。得られた単結晶について放射光X線源（SPring-8）を用いて回折データ収集を行い、以前の構造モデル（Tn46KおよびTn52K）を用いた分子置換法により立体構造を決定した。

C. 研究結果

今回全長ヒト心筋TnIを含む三量体コアドメインTn58Kを用いて新たな結晶化スクリーニングを行い、2003年に報告した条件とは全く異なる2条件で合計3種類の新規の結晶を得ることに成功した。この内の1つ（ここでは結晶3と呼ぶ）は結晶化条件と用いたTnIコンストラクトは異なるものの、2003年に報告した結晶の一つ（Tn52k）とほぼ同一の結晶格子を持ち、実際の構造解析においてもほぼ同一の結果を得た（Tn52Kで観測された以上の構造情報を得ることは出来なかった）。一方、残り2つの内の一つ（結晶2と呼ぶ）については3Å分解能の結晶データを用いて精密化を行った。結晶2は単位格子にTn2分子が存在し、それぞれ独立に構造決定した。また、残りの

結晶（結晶１）は含水量が約43％と少なく（以前の、Tn52K、Tn43Kはそれぞれ約51％）、結晶格子も小さく、回折分解能も高かった。この結晶１について構造解析を行い、2Å分解能までの回折データを使いて構造精密化を行うことに成功した（前回の構造解析ではTn46KおよびTn52Kについてそれぞれ2.6Åおよび3.3Å分解能であった）。これにより分子を構成する各原子位置をこれまでより高い精度で決定することが出来た。結晶1には単位格子にTn1分子が含まれていたため、今回結晶１，２の二つより計３分子の新たなヒト心筋トロポニン・コアドメインの構造決定を行ったことになる。2003年の構造解析４分子と合わせ合計７分子の独立した結晶構造を自分たちで得ることが出来た。

D. 考察

今回新たに得られた構造および以前の構造を合わせて比較することにより、分子内に存在する可動領域を新たに同定することが出来た。PKAリン酸化部位については残念ながらいずれの分子においても明瞭な電子密度図が得られず、生理的に重要であろう新たな発見は得られなかった。

E. 結論

ヒト心筋トロポニン三量体コアドメインの新規結晶構造の決定を行った。画期的な知見は得ることが出来なかったが、分子内に存在する可動領域を新たに明らかにすることが出来きた。また、今回２Å分解能のデータを用いることが出来、これにより原子位置座標の精度が非常に高い構造モデルを得ることに成功した。このモデルは今後トロポニンをターゲットとしたインシリコ・ドラッグディスカバリーを進める上では非常に有効な構造基盤となるであろう。

F. 研究発表

（研究業績「欧文」）

【総説】

1. Takeda S. "Three-dimensional domain architecture of the ADAM family proteinase." *Semin Cell Dev Biol* (in press)

【著書】

1. Takeda S. "VAP1: snake venom homolog of mammalian ADAMs." In: Messerschmidt A, editor. *Handbook of Metalloproteins*: John Wiley & Sons, Inc. (2008)

【原著論文】

1. H.Obata, Y.Sakai, S.Ohnishi, S.Takeshita, H.Mori, M.Kodama K.Kangawa, Y.Aizawa, N.Nagaya: Single Injection of a Sustained-release Prostacyclin Analog Improves Pulmonary Hypertension in Rats. : Am J Respir Crit Care Med. 2008; 177: 195-201
2. T.Yada, H.Shimokawa, K.Morikawa, A.Takaki, Y.Shinozaki, H.Mori, M.Goto, Y.Ogasawara, F.Kajiya: Role of Cu,Zn-SOD in the Synthesis of Endogenous Vasodilator Hydrogen Peroxide during Reactive Hyperemia in Mouse Mesenteric Microcirculation in Vivo. : Am J Physiol Heart Circ Physiol. 2008; 294: H441-H448
3. E.Sato, H.Obara, T.Enomoto, E.Tanaka, H.Mori, T.Kawai, T.Ichimaru, A.Ogawa, S.Sato, K.Takayama, J.Onagawa: X-ray Spectra from a Brass-target Plasma Triode: Jpn. J. Med. Phys. 2008; 27(4): 163-171
4. Y.Sato, E.Sato, S.Ehara, T.Enomoto, E.Tanaka, H.Mori, T.Kawai, A.Ogawa, S.Sato, J.Onagawa: Magnification K-Edge Angiography Utilizing 100-μm-Focus Tungsten Tube and Gadolinium-Based Contrast Media: Jpn. J. Appl. Phys. 2008; 47(6): 4772-4776
5. H.Matsukiyo, M.Watanabe, E.Sato, A.Osawa, T.Enomoto, J.Nagao, P.Abderyim, K.Aizawa, E.Tanaka, H.Mori, T.Kawai, S.Ehara, S.Sato, A.Ogawa, J.Onagawa: X-ray fluorescence camera for imaging of iodine media in vivo: Radiol Phys Technol. 2009; 2: 46-53"
6. A.Osawa, M.Watanabe, E.Sato, H.Matsukiyo, T.Enomoto, J.Nagao, P.Abderyim, K.Aizawa, E.Tanaka, H.Mori, T.Kawai, S.Ehara, S.Sato, A.Ogawa, J.Onagawa: Embossed radiography utilizing energy subtraction: Radiol Phys Technol. 2009; 2: 77-86"

【学会発表】

1. O.Ishida, I.Hagino, N.Nagaya, T.Shimizu Y.Sawa, H.Mori, T.Yagihara: Adipose-Derived Stem Cell Sheet Transplantation Therapy for Failured Heart:

第73回日本循環器学会総会・学術集会. 2009

2. T.Fujii, N.Fukuyama, Y.Ikeya, E.Tanaka, T.Sekka, Y.Shinozaki, K.Yamada, K.Umetani, K.Hyodo, E.Sato, K.Fukushima, T.Tanabe, H.Mori: Development of Microangiographic Systems for Visualization, Quantification and Therapeutic Evaluation of Angiogenic Vessels: The 11th International Symposium on Anti-Angiogenic Agents. ANGIO 2009, San Diego, (United States)
3. O.Ishida, I.Hagino, N.Nagaya, T.Shimizu, Y.Sawa, H.Mori, T.Yagihara, : Adipose-Derived Stem Cell Sheet Transplantation Therapy on Swine Chronic Heart Failure Model : Scientific Sessions 2008, American Heart Association
4. T.Yada, H.Shimokawa, O.Hiramatsu, Y.Shinozaki, H.Mori, M.Goto, Y.Ogasawara, F.Kajiya, : Crucial Role of Hydrogen Peroxide as an Endogenous EDHF during Acute Coronary Occlusion and Injection of Erythropoietin in Canine Coronary Native Collateral Microcirculation in Vivo, : Scientific Sessions 2008, American Heart Association
5. K.Yamada, R.Kuroda, H.Toyokawa, H.Ikeura-Sekiguchi, M.Yasumoto, N.Sei, H.Ogawa, M.Koike, R.Suzuki, F.Sakai, K.Mori, H.Mori, N.Fukuyama, E.Sato: Development of advanced quantum-beam sources and their applications as sophisticated imaging tools: Compton Sources for X/gamma Rays: Physics and Applications: 2008 in Italy
6. H.Mori, N.Fukuyama, Y.Ikeya, T.Fujii, N.Nagaya, Y.Miyahara, O.Ishida, S.Takeda: CONTRIBUTIONS OF NANOTECHNOLOGY TO CARDIOVASCULAR REGENERATIVE MEDICINE: Fourth Annual Meeting of American Academy of Nanomedicine. 2008

（研究業績「和文」）

【総説】

1. 荒木聡彦、五十嵐智子、武田壮一「血管内被細胞の破壊毒素：明らかになったADAM型細胞表面プロテアーゼの構造」表面 46(4), 24-33 (2008)

【学会発表】

1. 武田壮一、五十嵐智子、盛英三「ラッセルクサリヘビ由来血液凝固第X因子活性化プロテアーゼRVV-Xの結晶構造」、第8回日本蛋白質科学会年会、タワーホール船堀（東京）、2008.6（ポスター発表）
2. 武田壮一「蛇毒ホモログの結晶構造から見えてきたADAMファミリープロテアーゼの立体構造と作用機構」、シンポジウム「膜近傍におけるプロテオリシス」、第60回日本細胞生物学会年会、パシフィコ横浜、2008.6（招待講演）
3. 武田壮一「蛇毒高分子量メタロプロテアーゼの結晶構造と作用機構」、第55回毒素シンポジウム、ラフォーレ山中湖（山梨県）、2008.7（招待講演）
4. 武田壮一「発生・分化・病態に関わるADAMプロテアーゼ - 出血蛇毒素の結晶構造から見えてきたADAMの作用機構」、シンポジウム「生体分子による生物間の攻撃と防御」、東京大学弥生講堂・一条ホール、2008.11.8 (招待講演)
5. 武田壮一「心筋トロポニン三量体コアドメインの新規結晶構造と構造比較」、生体運動研究合同班会議、東京大学数理科学研究科・大講義室、2009.1.10 (口頭発表)
6. 石田治、宮原義典、永谷憲歳、盛英三「重症心不全に対する脂肪組織由来幹細胞シート移植治療法の開発」、第8回日本再生医療学会、2009

厚生科学研究費補助金　（医療機器開発推進研究事業）
ナノ分子イメージングを活用した次世代創薬アプローチ
分担研究報告書
次期治療標的タンパクの構造解析－２

分担研究者　増田　道隆　　国立循環器病センター研究所循環器形態部室長

研究要旨：循環器疾患、脳神経疾患等の制圧のためにナノテクノロジーを駆使して、治療法の開発を推進することを目的とする。本分担研究では、分子の構造決定に基づく創薬を目指した研究を行う。本年度も引き続き、脂質結合・変形活性をもつ共通のドメイン構造を有する細胞内情報伝達分子タンパク群（BARドメインスーパーファミリータンパク質）の構造および機能相関を解析する。これを、基盤情報として次世代創薬に貢献する。

A. 研究目的

脂質膜結合・変形タンパク質

生体膜のリモデリングは、膜輸送や飲・食作用、細胞やオルガネラの形状形成などの基盤をなす重要な細胞活性である。この活性は細胞骨格と膜変形分子の共同作用として実現されている。アクチン細胞骨格の制御に中心的な役割を果たしているRhoファミリー低分子GTP結合タンパク質のエフェクター分子の中に、アクチン細胞骨格制御活性とともに脂質膜結合・変形活性をもつ新規のタンパク質ファミリー（BARドメインスーパーファミリー）に属する分子I-BARファミリーがあることが明らかにされ、生体膜のダイナミックスを調整する分子として注目を集めている。I-BARの代表といえるIRSp53やBARドメインスーパーファミリーの構造研究は、生体膜のダイナミックスの制御をターゲットとした次世代創薬の可能性を開くものである。これらのタンパク質の分子機能の詳細を明らかにするため、タンパク結晶構造解析に取り組み、構造を基にしたデザイン変異体の機能解析から脂質膜変形能の分子的基盤を解明する。今年度はFerを主たるターゲットとして研究を進めた。

Ferは SH3ドメインを持たない代わりに、脂質膜結合・変形ドメイン（F-BARドメイン）を持つ特異な非受容体型のチロシンキナーゼである。Ferはユビキタスに発現して細胞接着制御に関わり、特に内皮細胞では接着分子のリン酸化を介して透過性の制御に関わる。我々は、内皮細胞の細胞間接着分子PECAM-1のキナーゼとしてFerを同定している。また、Ferは一部の癌の増悪化にも関係することが知られている。Ferを強制発現させても細胞質に存在することから、FerのF-BARドメインは活性が負に制御されていることが考えられる。逆にキナーゼ活性はF-BARドメインにより負に制御されているとの報告がある。脂質膜結合活性や、ドメイン間制御の詳細を明らかにするため、F-BARドメインおよび全長のタンパク結晶構造解析に取り組んだ。

B. 研究方法

IRSp53の脂質膜結合ドメインと、IP3などの脂質へ

ッドグループとの共結晶を作製し、X線回折法により構造を決定する。また、多数のトリプトファン変異体を作成し、FRET解析により、脂質膜結合サイトの情報を得る。Ferキナーゼの全長およびF-BARドメインの結晶を作製し、X線回折法により構造を決定する。また、構造に基づくデザイン変異体を多数作成し、in vivo, in vitroにおける機能解析により膜変形能の部域特異性についての情報を得る。

C. 研究結果

研究結果のうち、結晶構造解析については心臓生理部・武田室長およびペン-アマー室長との共同研究である。

(1) IRSp53

既に報告したIRSp53の脂質結合ドメインの結晶構造（分解能2.0Å）を用いて、分子置換法によりIP3との共結晶2種類の結晶構造解析を行なった。しかし分解能が足りず、IP3の位置決定に至らなかった。トリプトファン変異体によるリポソーム結合解析では、これまでの脂質膜変形モデルでは説明できないデータがでており、脂質膜変形の新しい機構を提案すべく研究を進めている。

(2) Fer

F-BARドメインの結晶構造解析に成功した。構造を基にした多数の変異体をデザインし、それらの脂質膜結合・変形活性を解析した。その結果、Ferの低い脂質膜結合・変形活性は、C-末側のSH2-キナーゼドメインによる負の制御を受けているためではなく、それ自体の活性が極めて低いことによることが示唆された。また、F-BARドメインのどの部域の正電荷が膜結合に重要であるかを示唆する知見を得た。

全長については、大腸菌による効率的なタンパク発現に成功し、結晶化条件をスクリーニングしている。

D. 考察

Ferキナーゼの結晶構造の解明により、Ferファミリーキナーゼの特異的性質を明らかにするとともに、脂質結合・変形活性がどのように遮蔽されているか、逆に、どのようにしたら発揮されるのかについて示唆を得ることができた。さらに研究を進め、局在とキナーゼ活性の制御メカニズムの詳細を明らかにすることにより、内皮細胞の透過性制御や機械刺激受容を調節する薬剤の開発につながる可能性がある。またこれらの研究は、新たな細胞生物学の研究領域の創成に資する。

E. 結論

I-BARやF-BARの構造決定を行ない、生体膜のダイナミックスの制御をターゲットとした次世代創薬や新研究領域創成の手がかりをつかんだ。

F. 研究発表

（研究業績「欧文」）

【原　著】

Komi Y, Suzuki Y, Shimamura M, Kajimoto S, Nakajo S, Masuda M, Shibuya M, Itabe H, Shimokado K, Oettegen P, Nakaya K, Kojima S: Mechanism of inhibition of tumor angiogenesis by beta-hydroxyisovalerylshikonin. Cancer Sci. 100 (2): 269-277, 2009.

H. 知的財産権の出願・登録

特になし

厚生科学研究費補助金 （医療機器開発推進研究事業:ナノメディシン研究）
分担研究報告書

ナノ分子機能イメージングを活用した次世代創薬アプローチ

分担研究者 国立循環器病センター研究所循環器形態部長 望月直樹

研究要旨　低分子量GTP結合蛋白質が血管新生・血管老化の調節に重要である。ナノ分子イメージングによる生体内での機能のイメージングを行う目的で動物個体のゼブラフィッシュを用いて血管新生と低分子量GTP結合蛋白質の可視化を行うための実験系・評価系を構築した。

A. 研究目的

血管新生、血管老化における低分子量GTP結合蛋白質の制御機構についての研究を行い、これらの分子を介した情報伝達系を制御可能な薬剤の開発のためのスクリーニング系の構築を目指した。これまで低分子量GTP結合蛋白質の活性化を可視化する系を構築しており、この分子プローブを用いたスクリーニング系の開発に努力してきた。今年度は、生体での低分子量GTP結合蛋白質の活性化を可視化する生物個体の作製と、血管構築を可視化できる個体であることの両方の条件をみたすゼブラフィッシュの作成を試みた。分子の機能イメージングとともに、開発薬剤の生体での効果判定に利用可能である個体の作成を目指した。

B. 研究方法

プラスミド: トランスポゾンによるDNAのゼブラフィッシュゲノムへのDNA挿入のための実験系に用いるプラスミドを構築した。プラスミドは血管内皮細胞特異的に発現する転写因子Fliのプロモーター用いて、低分子量GTP結合蛋白質の活性化を可視化するRaichu (Ras and interating molecule chimeric unit)をTol2で挟み込むDNAとなるように設計した(図1参照)。このプローブはYellow Fluorescnet protein (YFP) とCyan fluorescent protein (CFP)の間に低分子量GTP結合蛋白質とその標的分子の低分子量GTP結合蛋白質結合ドメインを挿入したキメラ分子となっている。

ゼブラフィッシュ: 野生型ゼブラフィッシュはストレインABを用いた。通常飼育で、夜ー昼サイクルを厳密に管理し、採卵を行った。
受精卵へのインジェクション: 実体顕微鏡下で、1細胞期に、上記のように作製したプラスミドをDNAのまま、またトランスポゾンをmRNAの状態でマイクロインジェクションで注入した。

蛍光タイムラプスイメージング:
体節間を走行する血管intersomitic vessel (ISV)が顕微鏡で観察可能となる授精後24時間から数時間かけて、倒立型の共焦点レーザー顕微鏡で蛍光蛋白質の発現を解析して血管構築のYFPによる可視化との低分子GTP結合蛋白質の活性化によるYFP-CFP間のfluorescent resonance energy transfer (FRET)の検出が行えるか否かを検討した。

C. 研究結果

プラスミドの構築:
低分子量GTP結合蛋白質の生体内可視化のために、まずRhoファミリー分子RhoA, Rac, Cdc42の可視化プローブをベクター内に挿入して、血管内皮細胞で特異的に発現するようなプラスミドを構築した。実際、トランスポゾンmRNAと一緒にインジェクションした個体では、YFPの蛍光が観察できたことから、世代を越えて挿入遺伝子が、継代されれば、目的の分子可視化ゼブラフィッシュの樹立になる。

FRETプローブの発現確認:
低分子量GTP結合蛋白質のFRETプローブがゼブラフィッシュで発現可能かいなかは、pCS2ベクターにFRETプローブcDNAを発現させ、これからin vitroでmRNAを作製し、授精卵へのinjectionを行って蛍光を観察することで確認した。また、共焦点レーザー顕微鏡によってYFP/CFP のratio イメージが十分検出可能であることも確認した。

蛍光検出による血管形成過程の可視化:
受精卵の血管構築は3次元であるために、共焦点レーザー顕微鏡による時間・空間解像度が十分であるか否かを検討した。図に示すようにDorsal aorta からのISVの背側への血管の新生が十分可視化できることが確認できた。また、空間解像度の問題もfilopodiaが十分観察できるだけの解像度であり、今後のfilopodia

あるいは細胞の遊走時のRHoファミリー分子の活性化の可視化に十分たえられるだけの検出感度があった。

D.考察

血管発生時には血管内皮細胞内でのシグナル伝達の制御が重要であり血管内皮細胞内のシグナル伝達の可視化が、生体で可能になれば、血管新生の抑制を目指したあるいは血管新生を目指した治療法の開発につながると考える。

低分子量GTP結合蛋白質のRhoファミリー分子の活性化はとくに細胞の進展や、収縮制御を行っているために細胞の運動に不可欠である。これらの分子の生体での活性化をイメージングした研究はなく、本研究が目指すまさに分子の機能のイメージングである。本研究の重要性は、さらにこの機能のイメージングに、今後開発予定である血管新生抑制、あるいは血管新生促進作用のある薬剤の効果判定まで個体を用いることで可能となることである。

われわれは分子の可視化を生体で行うことをこれまでの目標にしてきたが、今後もさらに様々な分子プローブをゼブラフィッシュに導入して、薬剤の効果判定や、機能の解明に繋げていきたいと考える。動物個体を用いた有効性を実証し、個体を用いたスクリーニング系の開発につなげていく計画である。

D. 結論

薬剤のスクリーニングあるいは効果判定に役立つ動物個体になることを目指して、血管新生における低分子量GTP結合蛋白質の可視化ゼブラフィッシュを作製した。

F. 健健康危険情報

なし

G. 研究発表

（研究業績「英文」）

【原著】

(1) Fukuhara S, Sako K, Minami T, Noda K, Kim HK[3], KodamT, Shibuya M,Takakura N, Koh GY, and Mochizuki N. Differential function of Tie2 at cell-cell contacts and cell-substratum contacts regulated by angiopoietin-1. **Nat. Cell Biol.** 10: 513-526, 2008

(2) Koyama T, Nakaoka Y, Fujio Y, Hirota H, Nishida K, Sugiyama S, Okamoto K, Yamauchi-Takihara K, Yoshimura M, Mochizuki S, Hori M, Hirano T, Mochizuki N. Interaction of scaffolding adaptor protein Gab1 with tyrosine phosphatase SHP2 negatively regulates IGF-I-dependent myogenic differentiation via the ERK1/2 signaling pathway. **J. Biol. Chem.** 283:24234-24244

(3) Kidoya H, Ueno M, Yamada Y, Mochizuki N, Nakata M, Yano T, Fujii R, Takakura N. Spatial and temporal role of the apelin/APJ system in the caliber size regulation of blood vessels during angiogenesis. **EMBO J.** 27: 522-534, 2008

(4) Yasuda N, Miura S, Akazawa H, Tanaka T, Qin Y, Kiya Y, Imaizumi S, Fujino M, Ito K, Zou Y, Fukuhara S, Kunimoto S, Fukuzaki K, Sato T, Ge J, Mochizuki N, Nakaya H, Saku K, Komuro I. Conformational switch of angiotensin II type 1 receptor underlying mechanical stress-induced activation. **EMBO Rep** 9:179-186 (2008)

2. 学会発表

特になし。

H. 知的財産権の出願・登録状況

特になし。

別紙4

研究成果の刊行に関する一覧表

書籍

著者	論文タイトル	編集者	書籍名	出版社	出版地	出版年	ページ
Takeda S.	VAP1: snake venom homolog of mammalian ADAMs.	Messerschmidt A.	Handbook of Metalloproteins	John Wiley & Sons, Inc.	Chichester West Sussex UK	2008	1-15

原著論文

発表者	論文タイトル	発表誌	巻号	ページ	出版年
Nakamura, T.Y., Iwata, Y., Arai, Y., Komamura, K., Wakabayashi, S.	Activation of Na^+/H^+ exchanger 1 is sufficient to generate Ca^{2+} signals that induce cardiac hypertrophy and heart failure	Circ. Res.	103(8)	891-899	2008
Lu, Y., Pang, T., Wang, J., Xiong, D., Ma, L., Li, B., Li, Q., Wakabayashi, S.	Down-regulation of P-glycoprotein expression by sustained intracellular acidification in K562/DOX cells	Biochem. Biophys. Res. Commun.	377(2)	441-446	2008
Y. Izuhara, S. Takahashi, M. Nangaku, S. Takizawa, H. Ishida, K. Kurokawa, C. v. Y. d. Strihou, N. Hirayama and T. Miyata	Inhibition of Plasminogen Activator Inhibitor-1. Its Mechanism and Effectiveness on Coagulation and Fibrosis	Arterioscler. Thromb. Vasc. Biol.	28(4)	672-677	2008
T. Akimoto, H. Hara, T. Nakano and N. Hirayama	Crystal Structure of (4SR, 5RS)-5-(4-Cyanophenyl)-4-trimethylsilyl-3-methylisoxazoline	Anal. Sci.	24	x165-x166	2008
S. Soga, H. Shirai, M. Kobori and N. Hirayama	Chemocavity: specific concavity in protein reserved for the binding of biologically functional small molecules	J. Chem. Inf. Model.	48	1679-1685	2008
R. Tanaka and N. Hirayama	Crystal Structure of Benzethonium Chloride Monohydrate	Anal. Sci.	24	x163-x164	2008
R. Tanaka and N. Hirayama	Crystal Structure of Linezolid	Anal. Sci.	24	x43-x44	2008
R. Tanaka and N. Hirayama	Crystal Structure of Guanabenz Acetate	Anal. Sci.	24	x5-x6	2008

R. Ogawa, T. Fujino, N. Hirayama and K. Sakai	Practical resolution of racemic trans-2-benzylaminocyclohexanol with di-p-toluoyl-L-tartaric acid via diastereomeric salt formation based on the Pope and Peachey method	Tetrahedron Asymmetry	19(21)	2458-2461	2008
J. Goto, R. Kataoka, H. Muta and N. Hirayama	ASEDock-Docking Based on Alpha Spheres and Excluded Volumes	J. Chem. Inf. Model	48	583-590	2008
H. Obata, Y. Sakai, S. Ohnishi, S. Takeshita, H. Mori, M. Kodama K. Kangawa, Y. Aizawa, N. Nagaya	Single Injection of a Sustained-release Prostacyclin Analog Improves Pulmonary Hypertension in Rats	Am J Respir Crit Care Med.	177	195-201	2008
T. Yada, H. Shimokawa, K. Morikawa, A. Takaki, Y. Shinozaki, H. Mori, M. Goto, Y. Ogasawara, F. Kajiya	Role of Cu, Zn-SOD in the Synthesis of Endogenous Vasodilator Hydrogen Peroxide during Reactive Hyperemia in Mouse Mesenteric Microcirculation in Vivo	Am J Physiol Heart Circ Physiol	294	H441-H448	2008
E. Sato, H. Obara, T. Enomoto, E. Tanaka, H. Mori, T. Kawai, T. Ichimaru, A. Ogawa, S. Sato, K. Takayama, J. Onagawa	X-ray Spectra from a Brass-target Plasma Triode	Jpn. J. Med. Phys.	27(4)	163-171	2008
Y. Sato, E. Sato, S. Ehara, T. Enomoto, E. Tanaka, H. Mori, T. Kawai, A. Ogawa, S. Sato, J. Onagawa	Magnification K-Edge Angiography Utilizing 100-μm-Focus Tungsten Tube and Gadolinium-Based Contrast Media	Jpn. J. Appl. Phys.	47(6)	4772-4776	2008
H. Matsukiyo, M. Watanabe, E. Sato, A. Osawa, T. Enomoto, J. Nagao, P. Abderyim, K. Aizawa, E. Tanaka, H. Mori, T. Kawai, S. Ehara, S. Sato, A. Ogawa, J. Onagawa	X-ray fluorescence camera for imaging of iodine media in vivo	Radiol Phys Technol.	2	46-53	2009
A. Osawa, M. Watanabe, E. Sato, H. Matsukiyo, T. Enomoto, J. Nagao, P. Abderyim, K. Aizawa, E. Tanaka, H. Mori, T. Kawai, S. Ehara, S. Sato, A. Ogawa, J. Onagawa	Embossed radiography utilizing energy subtraction	Radiol Phys Technol.	2	77-86	2009

Komi Y, Suzuki Y, Shimamura M, Kajimoto S, Nakajo S, Masuda M, Shibuya M, Itabe H, Shimokado K, Oettegen P, Nakaya K, Kojima S	Mechanism of inhibition of tumor angiogenesis by beta-hydroxyisovalerylshikonin	Cancer Sci.	100(2)	269-277	2009
Fukuhara S, Sako K, Minami T, Noda K, Kim HK3, KodamT, Shibuya M, Takakura N, Koh GY, and Mochizuki N.	Differential function of Tie2 at cell-cell contacts and cell-substratum contacts regulated by angiopoietin-1	Nat. Cell Biol.	10	513-526	2008
Koyama T, Nakaoka Y, Fujio Y, Hirota H, Nishida K, Sugiyama S, Okamoto K, Yamauchi-Takihara K, Yoshimura M, Mochizuki S, Hori M, Hirano T, Mochizuki N.	Interaction of scaffolding adaptor protein Gab1 with tyrosine phosphatase SHP2 negatively regulates IGF-I-dependent myogenic differentiation via the ERK1/2 signaling pathway	J. Biol. Chem.	283	24234-24244	2008
Kidoya H, Ueno M, Yamada Y, Mochizuki N, Nakata M, Yano T, Fujii R, Takakura N.	Spatial and temporal role of the apelin/APJ system in the caliber size regulation of blood vessels during angiogenesis	EMBO J.	27	522-534	2008
Yasuda N, Miura S, Akazawa H, Tanaka T, Qin Y, Kiya Y, Imaizumi S, Fujino M, Ito K, Zou Y, Fukuhara S, Kunimoto S, Fukuzaki K, Sato T, Ge J, Mochizuki N, Nakaya H, Saku K, Komuro I.	Conformational switch of angiotensin II type 1 receptor underlying mechanical stress-induced activation	EMBO Rep	9	179-186	2008

総説

発表者	論文タイトル	発表誌	巻号	ページ	出版年
中村(西谷)友重、古林創史、久光　隆、岩田裕子、若林繁夫	Na^+/H^+交換輸送体：機能調節と薬物標的としての意義	遺伝子医学	MOOK12	255-261	2009
Takeda S.	Three-dimensional domain architecture of the ADAM family proteinase	Semin Cell Dev Biol	(in press)	1-7	2008
荒木聡彦、五十嵐智子、武田壮一	血管内被細胞の破壊毒素：明らかになったADAM型細胞表面プロテアーゼの構造	表面	46(4)	24-33	2008

VAP1 – snake venom homolog of mammalian ADAMs

Soichi Takeda

Department of Cardiac Physiology, National Cardiovascular Center Research Institute, Osaka, Japan

FUNCTIONAL CLASS

Enzyme; monozinc endopeptidase; a P-III class snake venom metalloproteinase (SVMP); a member of the reprolysin/adamalysin/ADAM (a disintegrin and metalloproteinase) family; clan MA(M) > family M12B > M12.186 (MEROPS classification, http://merops.sanger.ac.uk/).

OCCURRENCE

Vascular-apoptosis-inducing protein-1 (VAP1) is a P-III class SVMP that was isolated from western diamondback snake *Crotalus atrox* venom as a factor that induces apoptosis in cultured vascular endothelial cells (VECs).[1,2] Similar apoptotic SVMPs have been isolated from other hemorrhagic snake venoms.[3–8] SVMPs are classified into various groups (P-I to P-IV) according to their domain organization.[9,10] P-III SVMPs are composed of metalloproteinase (M), disintegrin-like (D), and cysteine-rich (C) domains, and display more potent hemorrhagic activity than P-I SVMPs, which contain only an M domain. In addition to apoptotic toxins, snake venoms contain a number of other SVMPs that play key roles in the pathologies associated with

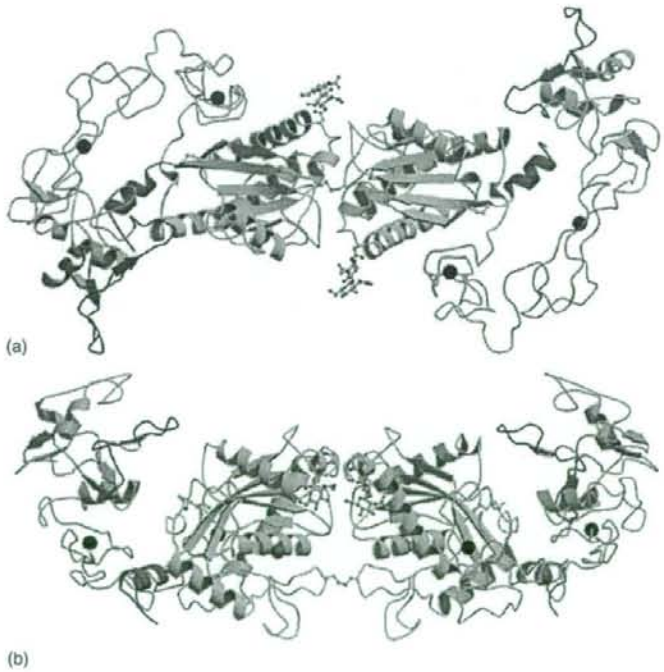

3D Structure Ribbon diagram of VAP1, viewed from the dimer axis (a) and from the direction perpendicular to the dimer axis (b), PDB code 2ERO. The structural subsegments are represented in different colors as follows: the h0-helix, M domain, linker, D_s, D_a, C_w, C_h segments, and HVR are shown in red, yellow, gray, cyan, pink, gray, light green and blue, respectively. Carbohydrate moieties linked to Asn218 are in ball-and-stick representation. The catalytic zinc ions and the calcium ions are represented by red and black spheres, respectively. Figures were generated using the MOLSCRIPT[83] and RASTER3D[84] programs.

envenoming, such as hemorrhage, edema, inflammation, and necrosis.[9–11] Mammalian ADAM family proteins are phylogenically related to P-III SVMPs and have a homologous metalloproteinase/disintegrin/cysteine-rich (MDC) domain architecture.[10,12] ADAMs and SVMPs, together with ADAMTSs (ADAM with thrombospondin type-1 motif),[13,14] constitute the adamalysin/reprolysin/ADAM subgroup of the metzincin clan of zinc proteinases.[15,16] ADAMs are primary type-I transmembrane proteins. In addition to the amino-terminal MDC domains, ADAMs have a transmembrane segment and a cytoplasmic region in their carboxy terminus.[12,17,18] The canonical ADAMs (see below) also have an epidermal growth factor (EGF)-like domain between the C domain and the transmembrane segment. ADAMs are widely expressed in multicellular organisms, including humans, mice, *Drosophila melanogaster*, and *Caenorhabditis elegans*. ADAMs are also expressed in *Schizosaccharomyces pombe* (but not in *Saccharomyces cerevisiae*).[19] Some ADAMs have alternatively spliced secreted forms in addition to the prototype transmembrane form.[20,21] There are 20 genes that encode human ADAMs and 37 genes that encode mouse ADAMs. The ADAMTS family is a branch of ADAMs, and constitutes a group of secreted proteinases that are expressed in a broad spectrum of species, ranging from humans to worms.[22] There are 19 known ADAMTS proteinases in vertebrates. A schematic representation of the domain structure of representatives of the adamalysin/reprolysin/ADAM family of proteins is shown in Figure 1.

BIOLOGICAL FUNCTION

SVMPs circulate within envenomed animals and are primarily responsible for local and systemic bleeding.

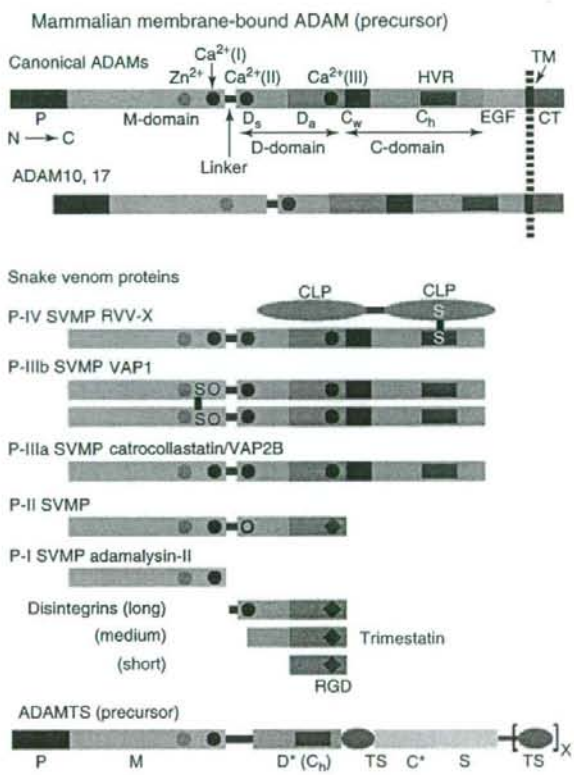

Figure 1 Schematic representation of the domain structures of ADAM/adamalysin/reprolysin family of proteins. Each domain or subsegment is colored as follows: the prodomain (Pro), transmembrane (TM), cytoplasmic region (CT), C-type lectin-like domain (CLP), thrombospondin type-1 domain (TS), and spacer (S) domain are in black, black, gray, brown, gray, and light green, respectively. The use of disintegrin-like (D) in the nomenclature of ADAMTS is a misnomer[23] as the D domain in ADAMTS-1 appears to be very similar in structure to the C_h segment of VAP1. Thus, the D domain of ADAMTSs is represented as the C_h segment. The C domain in ADAMTSs has no sequence homology to ADAMs, and is represented by a distinct color.

Some SVMPs do not possess hemorrhagic activity, but have other diverse functions attributable to them, such as fibrinogenase, prothrombin activating, or plate aggregation inhibitor activities.[10] VAP1 induces cell death in VECs in culture with the characteristic features of apoptosis, including fragmentation of cells and cleavage of DNA into a characteristic ladder pattern upon electrophoresis.[2] VAP1-induced apoptosis is dependent on its catalytic activity,[24] is inhibited by antibodies to integrins α3, α6, β1, and CD9 (cluster of differentiation antigen-9),[25] and involves activation of specific caspases.[26] However, the physiological target(s) of VAP1 and the underlying mechanism of VAP1-induced apoptosis remain elusive.

The first mammalian ADAMs, termed *fertilin* (hetero dimer of α- (ADAM1) and β-chain (ADAM2)), was identified in 1992 as surface molecules on sperm cells that are essential for fertilization.[27] Meltrins α (ADAM12), β (ADAM19), and γ (ADAM9) were isolated as molecules involved in myogenesis.[28] The best-characterized *in vivo* activity of mammalian ADAMs is their ectodomain sheddase activity. ADAM17 (tumor necrosis factor converting enzyme or TACE) was initially identified as the physiological convertase for tumor necrosis factor (TNF)-α.[29,30] ADAM10 (kuzbanian), which dictates the lateral inhibition of *Drosophila* neurogenesis,[31] releases Notch ligand delta[32] and Notch.[33] ADAM-mediated shedding can be activated by ligands for G-protein-coupled receptors (GPCRs). ADAMs have also been implicated in mitogenic events associated with EGF receptor transactivation by GPCRs.[34–36] However, in contrast to SVMPs and ADAMTSs, all of which are proteolytically active, only 60% of mammalian membrane-bound ADAMs contain the signature catalytic site motif HEXXHXXGXXHD (where X denotes any amino acid). The function of the proteinase-inactive ADAMs remains unclear. Aside from sheddase activity, ADAMs function in cell–cell and cell–matrix adhesion. The domains that are carboxy terminal to the M domain of ADAMs have been shown to exhibit adhesive activities in tissue culture.[37–39] ADAMs have been associated with numerous disease conditions including rheumatoid arthritis, Alzheimer's disease, heart disease, and cancer.[36,40,41] ADAM33 has been genetically linked to asthma and bronchial hyperresponsiveness in Caucasians.[42]

Disintegrins are small proteins (40–90 amino acids) that are generated, albeit not exclusively,[43] by proteolytic processing of larger precursor P-II SVMPs that are composed of M and D domains.[44,45] They typically possess an Arg-Gly-Asp (RGD) recognition sequence on an extended loop (disintegrin loop) that has been shown to inhibit platelet aggregation *via* integrin binding.[46,47] ADAMs are unique among the cell-surface proteins in that they possess a disintegrin-like sequence, which suggests that integrins are common receptors for ADAMs.[12,18,27,48] However, the RGD sequence in the ADAMs disintegrin-loop is usually replaced by XXCD, and therefore, the adhesive properties of the D domain are controversial.

AMINO ACID SEQUENCE INFORMATION

The VAP1 cDNA encodes a protein of 610 amino acid residues (EMBL database: AB042840). Mature VAP1 is a disulfide-bonded homodimer of polypeptide chains of 423 residues each. The signal sequence and the prodomain, which precede the M domain, are cleaved by posttranslational processing, and the mature protein contains only the MDC domain. The MDC domains of human ADAMs exhibit 30–40% sequence identity with VAP1.[49]

The prodomain of VAP1 contains a cysteine-containing sequence, PKMCGVT, which is thought to maintain the proteinase in a latent state, and is activated by a cysteine-switch mechanism.[50] The cysteine-containing sequence is conserved among the adamalysin/reprolysin/ADAM family proteins and the matrix metalloproteinases (MMP) of the metzincin clan of metalloproteinases. The mechanism of removal of the prodomain of VAP1 has not been clarified. The activation of some ADAMs has been shown to involve their own proteinase activity, while the others are believed to be activated by proprotein convertases (e.g. furin) in the secretary pathway.

PROTEIN PRODUCTION, PURIFICATION, AND MOLECULAR CHARACTERIZATION

VAP1 can be purified from the lyophilized powder of *C. atrox* venom by conventional liquid chromatography.[51] In the amino terminus of the M domain, Glu184 is modified to its pyro-form, and a carbohydrate chain is linked to the residue Asn218.[49]

VAP1 has a unique dimeric structure, and most adamalysin/reprolysin/ADAM family proteins do not appear to form VAP1-type dimers, as they lack the consensus QDHSK sequence (residues 320–324 in VAP1) and Cys365.[49] The consensus sequence and a cysteine residue at this position are found in other apoptotic P-III SVMPs, such as HV-1 (habu snake vascular-apoptosis-inducing protein-1),[4] halysase,[5] and VLAIP (*Vipera lebetina* apoptosis-inducing protein).[6] The VAP1-type dimers are categorized as the P-IIIb subclass of SVMPs, to distinguish them from the monomeric P-IIIa SVMPs.[10]

METAL CONTENT AND COFACTORS

There are one zinc and two calcium ions bound per VAP1 monomer, as shown by X-ray crystallography.[49] On the basis of the structures of VAP1 and the related proteins, and amino acid sequence alignment, the canonical ADAM MDC domains contain one zinc ion and three calcium ions. No other cofactors are present.

ACTIVITY AND INHIBITION TESTS

VAP1 degrades fibrinogen *in vitro*,[24] although the cleavage site(s) has not been identified. After incubation with either ethylenediaminetetraacetic acid (EDTA) or ethyleneglycol bis (2-aminoethyl ether) tetraacetic acid (EGTA), the ability of VAP1 to degrade fibrinogen and induce apoptosis in VECs is severely impaired.[24] Hydroxamic acid derivatives, such as GM6001 has been given as (*N*-[(2*R*)-2-(hydroxamidocarbonylmethyl)-4-methylpentanoyl]-L-tryptophan methylamide) also inhibit VAP1-induced VEC apoptosis. Therefore, the metalloproteinase activity of VAP1 appears to be involved in the induction of apoptosis by VAP1. Most of the hemorrhagic SVMPs degrade basal membrane component proteins[11]; however, the degradation activity of VAP1 toward those proteins *in vitro* is very weak.

The 12 human ADAMs (ADAM8, 9, 10, 12, 15, 17, 19, 20, 21, 28, 30, and 33) contain a catalytic signature sequence (HEXXHXXGXXHD), and most of them (with the exception of ADAM20, 21, and 30) have been shown to be proteolytically active.[12,17,18]

X-RAY AND NMR STRUCTURES

The first member of the adamalysin/reprolysin/ADAM family of proteinases for which the X-ray structure was determined was adamalysin II, a P-I SVMP from *Crotalus adamantus*.[52,53] Since then, crystal structures of seven P-I SVMPs have been published.[54–60] The structures of several disintegrins have been determined by X-ray crystallography[61–63] and NMR.[64–68] Although the crystallization papers of two P-III SVMPs, Jararhagin from *Bothrops jararaca* and AaH-IV from *Agkistrodon acutus* venoms, are available,[69,70] the three-dimensional structures have not been reported. The structures of seven mammalian proteins are currently available – the M domains of human ADAM17[71] and ADAM33,[72] the DC domains of bovine ADAM10,[73] the M domain of human ADAMTS-5,[74] and the MD domains of human ADAMTS-1,[23] ADAMTS-4, and ADAMTS-5.[75]

VAP1 was the first P-III SVMP structure to be resolved by X-ray crystallography.[49] The crystal structures of VAP1 have revealed an MDC domain architecture, which is shared by the mammalian ADAMs. Crystal structures of three different crystal forms of catrocollastatin/VAP2B, an apoptotic, monomeric class (P-IIIa) of SVMP[3,7] that has platelet-aggregation inhibitory activity,[76] have been determined.[77] A comparison of the six catrocollastatin/VAP2B structures and the structures of VAP1 reveals a dynamic, modular architecture of the MDC domains that may be important for the functions of adamalysin/reprolysin/ADAM family proteins.[77] The third MDC-containing SVMP for which the crystal structure was solved is RVV-X,[78] an unusual metalloproteinase that belongs to the P-IV class of SVMPs. Two C-type lectin-like chains are added posttranslationally to the C domain of P-III class SVMPs.[10,79–81] Although no mammalian ADAM MDC-domain crystal structures are currently available, electron microscopy of negative-stained recombinant ADAM12 with its prodomain revealed a four-leaf-clover shape, in which three of the four leaves represented the MDC domains.[82] Table 1 summarizes the adamalysin/reprolysin/ADAM family proteins currently entered into the Protein Data Bank.

Crystallization

VAP1 was crystallized in two distinct crystal forms using the sitting or hanging drop vapor diffusion methods.[49,51] Crystals were obtained with a reservoir solution that contained 15% polyethyleneglycol (PEG) 8000 and 100 mM sodium cacodylate at pH 6.5, with (orthorhombic form) or without (tetragonal form) 20 mM cobaltous chloride hexahydrate. The orthorhombic crystals belonged to space group $P2_12_12_1$ with $a = 86.7$ Å, $b = 93.3$ Å, $c = 137.7$ Å and one VAP1 dimer in the asymmetric unit. The tetragonal crystals belonged to space group $P4_12_12$ with $a = b = 93.9$ Å, $c = 244.8$ Å and one VAP1 dimer per asymmetric unit. Inhibitor-bound crystals were prepared by adding GM6001 to the drop with the orthorhombic crystal at a final concentration of 0.33 mM, followed by a 12-h incubation. Native structures were determined from crystals in the two distinct space groups at 2.5 Å resolution, and GM6001-bound structure was determined at 3.0 Å resolution.[49]

Like other proteins, adamalysin/reprolysin/ADAM family proteins are more prone to crystallize with inhibitors, which not only increase the thermal stability of the proteins[74] but also provide additional contacts with neighboring molecules in the crystalline lattice.[51,77,78]

MDC domains form a 'C shape'

The MDC domain architecture of VAP1 is shown in 3D structure and Figure 2(a) and (b). The M domains in the dimer are related by a noncrystallographic twofold axis, such that their active sites point in opposite directions, and an interchain disulfide bridge is formed between symmetry-related Cys365 residues. Each monomer has an almost identical structure except for the subdomain orientations. The M domain is followed by the D domain, which is further divided into two structurally distinct subsegments, the 'shoulder' (D_s) and the 'arm' (D_a) segments. The D_s segment protrudes from the M domain close to Ca^{2+} binding site I (see below), opposite the catalytic zinc ion. The C domain is subdivided into 'wrist' (C_w) and 'hand' (C_h) segments. Because of the curved structure of the $D_s/D_a/C_w/C_h$ segments, with the concave surface facing

Table 1 Selection of the 3D structures of ADAM/adamalysin/reprolysin family proteins currently deposited in the PDB

Protein	Domains	Method	PDB code	Reference
Snake venom proteins				
VAP1	MDC (homodimer)	X ray	2ERO, 2ERP, 2ERQ	49
Catrocollastatin/VAP2B	MDC	X ray	2DW0, 2DW1, 2DW2	75
RVV-X (russellysin)	MDC + 2CLPs	X ray	2E3X	76
Adamalysin II	M (P-I SVMP)	X ray	1AIG, 2AIG, 3AIG	52, 53
Atrolysin C	M (P-I SVMP)	X ray	1ATL, 1HTD	54
Acutolysin A	M (P-I SVMP)	X ray	1BSW, 1BUD	55
BaP1	M (P-I SVMP)	X ray	1ND1	56
H2	M (P-I SVMP)	X ray	1WNI	57
TM-3	M (P-I SVMP)	X ray	1KUF, 1KUG, 1KUI, 1KUK	58
Acutolysin C	M (P-I SVMP)	X ray	1QUA	59
FII	M (P-I SVMP)	X ray	1YP1	60
Trimestatin	Disintegrin	X ray	1J2L	61
Schistatin	Disintegrin (homodimer)	X ray	1RMR	62
Disintegrin (*Echis carinatus*)	Disintegrin (heterodimer)	X ray	1TEJ	63
Disintegrin (*Echis carinatus*)	Disintegrin (homodimer)	X ray	1Z1X	Unpublished
Kistrin	Disintegrin	NMR	1N4Y	67
Rhodostmin	Disintegrin	NMR	2PJF	Unpublished
Echistatin	Disintegrin	NMR	1RO3, 2ECH	65
Flavoridin	Disintegrin	NMR	1FVL	66
Obtustatin	Disintegrin	NMR	1MPZ	64
Salmosin	Disintegrin	NMR	1L3X	68
Mammalian proteins				
ADAM33	M	X ray	1R54, 1R55	72
ADAM17 (TACE)	M	X ray	1BKC	71
ADAM10	DC	X ray	2AO7	73
ADAMTS-5	M	X ray	3B8Z	74
ADAMTS-1	MD*	X ray	2JIH, 2V4B	23
ADAMTS-4	MD*	X ray	2RJP, 3B2Z	75
ADAMTS-5	MD*	X ray	2RJQ	75

* The use of disintegrin-like (D) domain in the nomenclature of ADAMTS is a misnomer.[23] The D-domain in ADAMTSs appears no structural similarity to the D-domain of ADAMs and SVMPs, and thus is represented as "D*".

the M domain, the overall appearance of the MDC domains is a C-shaped configuration. The distal portion of the C_h segment comes close to and faces the catalytic zinc ion in the M domain.

Metalloproteinase domain

The VAP1 M domain has as an oblate ellipsoidal shape with a notch in its flat side that creates a relatively small 'lower' domain and an 'upper' main molecular body in the 'standard' orientation,[15,52,85] wherein the active-site cleft extends horizontally across the M-domain surface to bind peptide substrates from left to right (Figure 2b). The catalytic zinc atom is located at the bottom of the cleft. The amino-terminal upper domain has a central core consisting of highly twisted five-stranded β-sheets and five α-helices. The amino-terminal h0 helix located on the h5 helix is unique to VAP1, and is not found, to date, in the structures of other family members. The curved β-sheets are parallel, with the exception of s4-strand, which faces the active-site cleft, and is sandwiched between helices h2 and h4 on the concave side and helix h3 on the convex side. The short helix h1 is located at an edge of the β-sheet. A topology diagram of the M domain is shown in Figure 2(c). The secondary structural arrangement is similar to other metzincins, such as astacin[85] and human neurophil collagenase (MMP-8),[86] except for a large insertion of helix h3 and the loop between strand s2 and helix h3. This insertion contributes to calcium binding site I (see below), which is unique in the adamalysin/reprolysin/ADAM family proteinases. The carboxy-terminal lower domain consists of helix h5 and an irregularly folded region. This irregular region is presumably important for substrate recognition because it forms, in part, the wall of the S1′ crevice, contains the 'Met-turn', and is stabilized by two conserved disulfide bridges (Cys350–Cys374 and Cys352–Cys357). A third highly conserved disulfide bridge (Cys310–Cys390)

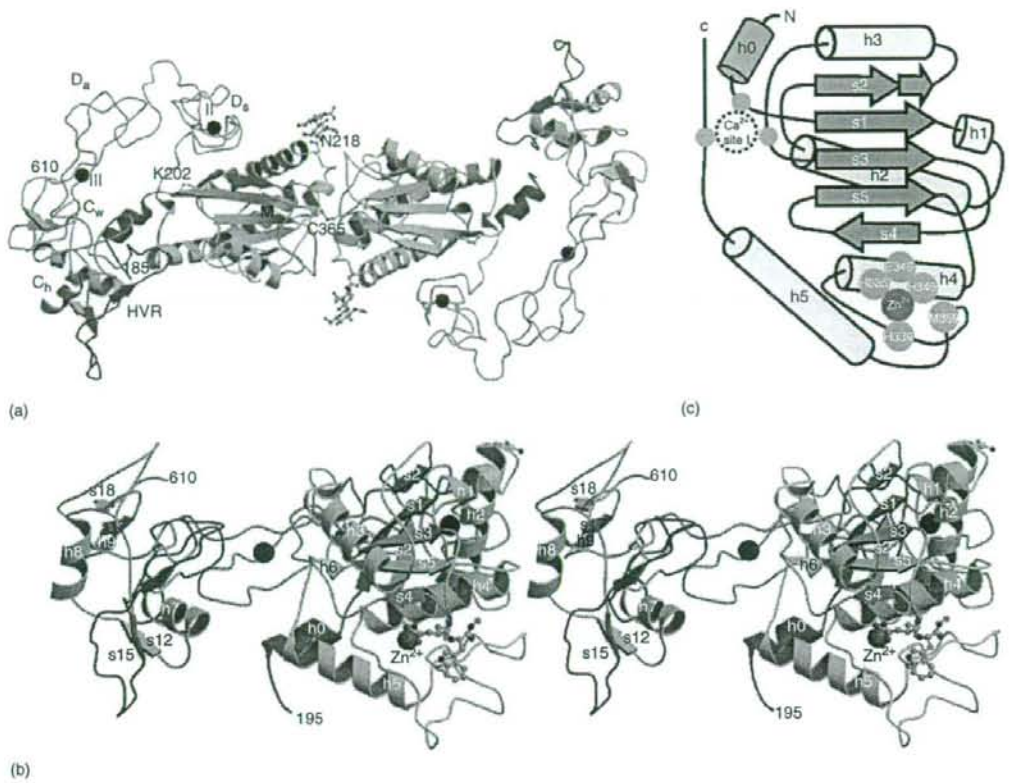

Figure 2 Ribbon structure of VAP1. (a) VAP1 dimer viewed from the twofold axis. The h0 helix, M domain, linker, D_s, D_a, C_w, C_h segments, and HVR are shown in red, yellow, gray, cyan, pink, gray, light green, and blue, respectively. Zinc and calcium ions are represented as red and black spheres, respectively. The carbohydrate moieties linked to Asn218 the calcium-mimetic Lys202 and bound GM6001 (in green) are in ball–stick representations; (b) stereo view of the VAP1 monomer in the standard orientation, nearly perpendicular to the view in (a); (c) topology diagram of the VAP1 M domain. Figures were generated using the MOLSCRIPT[83] and RASTER3D[84] programs.

connects the two subdomains close to Ca^{2+} binding site I. The M domain of VAP1 can be superposed with those of human ADAM33[72] and ADAM17[71] (Figure 3).

Arm structure

The VAP1 D domain is linked to the M domain by a short linker that allows variable orientation between the M domain and the D_s segment. The D_s and D_a segments consist largely of a series of turns and two short regions of antiparallel β-sheet, and constitute an elongated C-shaped arm structure together with the amino-terminal region of the C domain, the C_w segment (Figure 4(a)). The C_w segment consists of a pair of antiparallel β-strands and loops. It packs against the D_a segment on one side and against the carboxy-terminal β-sheet of the C_h segment on the other. There are three disulfide bridges in the D_s segment, three in the D_a segment, and one in the C_w segment. The subsegments are connected by single disulfide bridges. The number and spacing of the cysteine residues involved in these disulfide bridges are highly conserved among adamalysin/reprolysin/ADAM family proteins (Figure 4(c)).[10,44,49,77] Because there are few secondary structural elements, the disulfide bridges, together with bound calcium ions (see below), are essential for the structural rigidity of each segment of the C-shaped arm structure.

As predicted from its amino acid sequence, the structure of the D_a segment is similar to that of the RGD-containing disintegrin trimestatin (root mean square deviation (rmsd) of 1.24 Å),[61] with the exception of the disintegrin loop and the carboxy terminus of the D_a segment (Figure 4(b)). These two regions in disintegrins are highly mobile and are candidate sites for integrin binding.[65–67] Using isolated D domains or portions of them, numerous

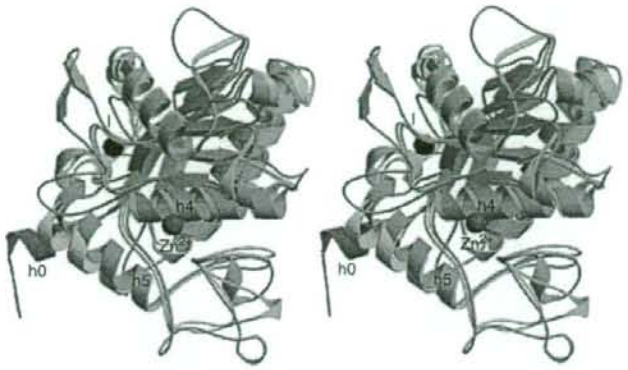

Figure 3 Stereo view of the superimposition of the M domains of VAP1 (yellow), ADAM33 (cyan), and ADAM10 (pink). The calcium ion bound to site I and the zinc ion in ADAM33 are represented by black and red spheres, respectively. The h0 helix in VAP1 is colored red.

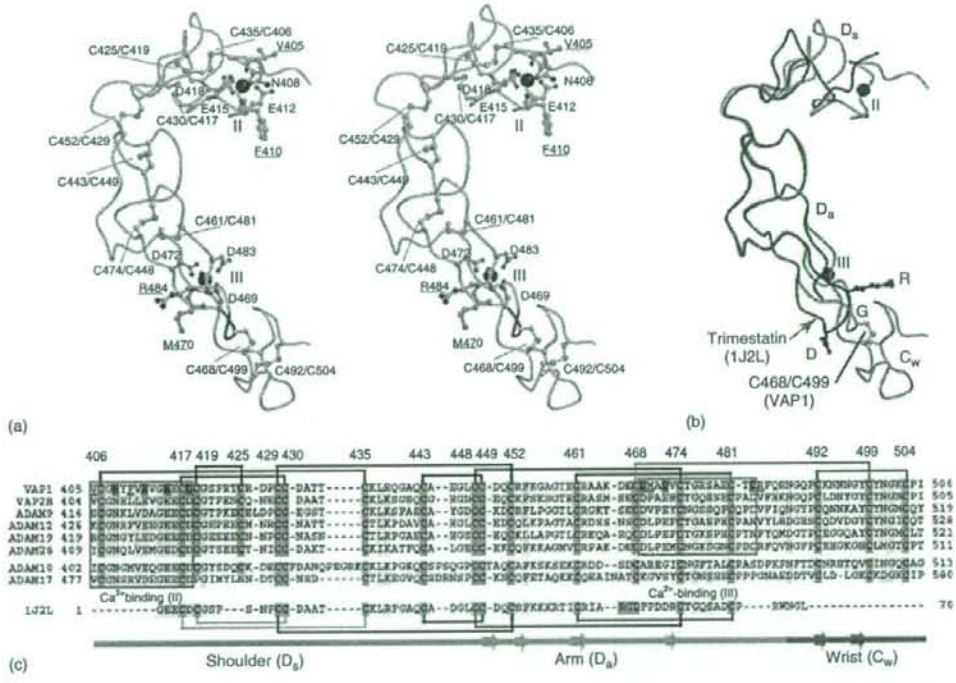

Figure 4 Arm structure of VAP1 (a) stereo diagram of the arm structure. The D_s, D_a, and C_w segments are in cyan, pink, and light green, respectively. The residues involved in calcium ion coordination and the disulfide bridges are shown in red and green, respectively. The carbonyl oxygen atoms of the residues that are involved in calcium coordination are underlined. Calcium ions are represented as black spheres. The disintegrin-loop (DECD) is in blue; (b) superimposition of the D_s segments of VAP1 and trimestatin (1J2L). Trimestatin and its RGD loop residues are shown in red and blue, respectively; and (c) amino acid sequence alignment of VAP1, trimestatin, and human ADAMs. The cysteinyl residues and conserved residues are shaded in pink and yellow, respectively. Disulfide bridges, secondary structures, and the boundary of the segments are shown schematically. The calcium binding sites are boxed in red, and the residues involved in calcium ion coordination are indicated. The National Center for Biotechnology Information (NCBI, http://www.ncbi.nlm.nih.gov/) accession numbers for the sequences are BAB18307 for VAP1, AAC59672 for VAP2B (catrocollastain/VAP2B), NP_003807 for ADAM9, AAC08703 for ADAM12, NP_075525 for ADAM19, NP_079496 for ADAM28, Z48579 for ADAM10, U69611 for ADAM17, and 1J2L for trimestatin. Figures were generated using the MOLSCRIPT[83] and RASTER3D[84] programs.

ADAMs, and P-III SVMPs have been shown to interact with integrins.[12,18,47,48] However, in VAP1, a bound calcium ion at site III forms a structural core that stabilizes the disintegrin-loop that is packed against the C_w segment. A disulfide bond (Cys468–Cys499) further stabilizes the continuous structure, which suggests that there is little intersegment flexibility. Cys468 is conserved among mammalian ADAMs and P-III SVMPs, which always contain a C domain. The structures of the DC domains of bovine ADAM10,[73] catrocollastain/VAP2B,[77] and RVV-X[78] also show a continuous D_a/C_w structure. These observations suggest that the disintegrin loop in ADAMs and P-III SVMPs is unavailable for protein binding due to steric hindrance.

Metal site geometries

Catalytic site (Zn^{2+})

VAP1 has a zinc-binding consensus sequence (HEXXHXXGXXH), which is characteristic of the metzincin superfamily.[15,16] The zinc ion is situated at the bottom of the catalytic cleft, and is tetrahedrally coordinated by the Nε2 atoms of the three consensus histidines, His335, His339, and His345, with bond distances of 2.0–2.2 Å. The coordination of the catalytic zinc atom is almost the same as in other members of this family. In GM6001-bound VAP1, the zinc ion is pentacoordinated by the two hydroxamate oxygen atoms and the Nε2 atoms of the three histidines (Figure 5).

Ca^{2+} binding site in the M domain (Ca^{2+} site I)

The MDC domain contains three potential Ca^{2+} binding sites. The structures of the M domain of ADAM33[72] and

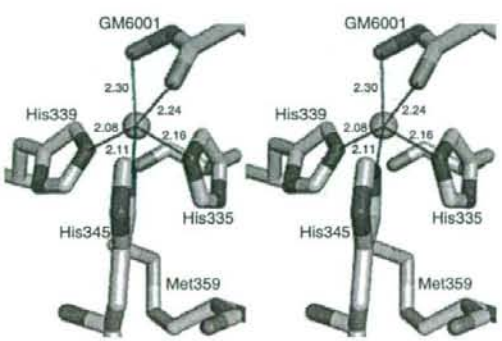

Figure 5 Stereo diagram of the catalytic zinc (pink sphere) of the VAP1–GM6001 complex (PDB code 2ERQ). The hydroxamic acid group of bound GM6001 and three histidine ligands are shown, along with the Zn–N/O distances (angstrom). The figure was generated using PyMOL.[87]

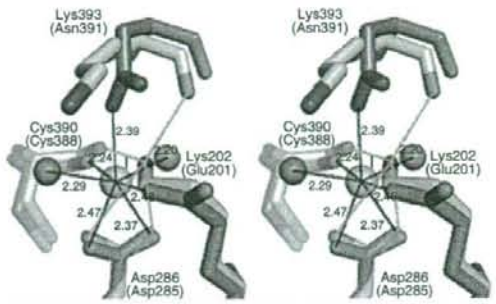

Figure 6 Stereo diagram of calcium binding site I of VAP1 (gray) superposed on that of catrocollastain/VAP2B (blue). The Ca^{2+}/N–O distances (angstrom) are indicated. The figure was generated using PyMOL.[87] The ammonium group of Lys202 in VAP1 occupies the position of the calcium ion in catrocollastatin/VAP2B.

of other P-I SVMPs[52,53,55] suggest that most ADAMs have a Ca^{2+} binding site (designated Ca^{2+} binding site I) that is in opposition to the active-site cleft close to the crossover point of the amino-terminal and carboxy-terminal segments of the M domain. In catrocollastatin/VAP2B, this Ca^{2+} ion is coordinated by the side chains of Asp285, Asn391, and Glu201, the backbone carbonyl oxygen of Cys388, and two water molecules in a pentagonal bipyramidal arrangement.[77] The three side chains that coordinate the Ca^{2+} ion are largely conserved among ADAMs and SVMPs. However, in VAP1, Glu and Asn are replaced by Lys202 and Lys392, respectively, and the distal ammonium group of Lys202 substitutes for the Ca^{2+} ion (Figure 6). Replacement of the calcium-coordinating glutamate residue with lysine is also observed in several ADAMs (e.g. human ADAMs16, 25, and 38–40). The high degree of conservation of residues involved in calcium binding and the presence of mimetic calcium binding might reflect the importance of this region for the structural link between the M and D_s domains. A protective role for calcium against auto proteolysis in the linker region has also been reported,[45,53,88] and the linker region is usually removed from P-I SVMPs posttranslationally.[89] ADAM17[71] and, presumably, ADAM10 do not possess this calcium binding site. These two ADAMs are not typical members of the mammalian family of ADAMs. They also lack Ca^{2+} binding site III, and lack an EGF domain.

Ca^{2+} sites in the D_s- and D_a segments

The structure of both the D_s and D_a segments revealed Ca^{2+} binding sites[49] that were not predicted by protein sequence. In the D_s segment, side-chain oxygen atoms of residues Asn408, Glu412, Glu415, and Asp418, and main-chain oxygen atoms of Val405 and Phe410 are

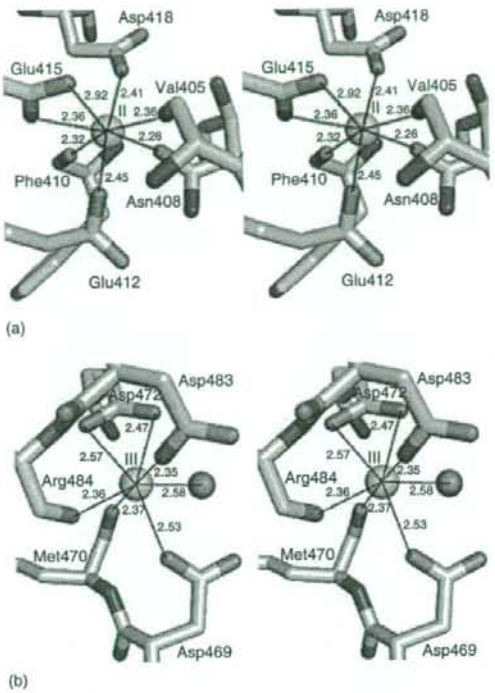

Figure 7 Stereo diagram of bound calcium ions in the (a) D_s segment (site II) and in the (b) D_a segment (site III) of VAP1. The Ca^{2+}–O distances (angstrom) are indicated. The figure was generated using PyMOL.[87]

involved in pentagonal bipyramidal coordination (hepta-coordination) of Ca^{2+} binding site II (Figure 7(a)). Of note, these residues are strictly conserved among all known mammalian ADAMs and P-III SVMPs.[49,77] Side-chain oxygen atoms of Asp469, Asp472, and Asp483, and the main-chain carbonyl oxygen atoms of Met470 and Arg484 coordinate the binding of a Ca^{2+} ion at the corners of a pentagonal bipyramid, and constitute Ca^{2+} binding site III in the D_a segment (Figure 7(b)). These residues are highly conserved among mammalian ADAMs, with the exception of ADAM10 and ADAM17.[49,77]

Hand (C_h segment) structure and hypervariable region (HVR)

The core of the carboxy-terminal region of the VAP1 C domain, the C_h segment, is an α/β fold structure that consists of two antiparallel β-strands packed against two of the three α-helices, and five disulfide bonds (Cys511–Cys561, Cys526–Cys572, Cys539–Cys549, Cys556–Cys598, and Cys592–Cys603) (Figure 8(a)). The C_h segment of VAP1 has a novel and unique fold with no structural homology to other known proteins, with the exception of the corresponding segment of ADAM10[73] and ADAMTS-1[23] (see below).

The loop encompasses residues 562–583, and extends across the central region of the C_h segment. It is the region in which the ADAM sequences are most divergent and variable in length (11–55 aa) (Figure 8(e)). We have designated this the hypervariable region (HVR).[49] In all the crystal forms of VAP1 and catrocollastatin/VAP2B, the HVR is involved in crystal packing, and forms a short antiparallel β-strand in the center that participates in a 'handshake' with the HVR of a neighboring molecule.[49,77] The structure of the HVR is stabilized mainly by interchain interactions. However, while there are no main chain–main chain hydrogen bonds between residues 574–584 and the remainder of the C_h segment, a water-mediated hydrogen bond network helps stabilize the HVR structure. Therefore, it appears that the HVR β-strand might be formed by an induced fit mechanism upon the association of the C_h segment, and that the conserved disulfide bridge (Cys526–Cys572) stabilizes the structure when the HVR is isolated in solution. Some ADAMs possess a putative fusion peptide sequence in this segment that is typical of viral fusion proteins[27,28]; however, its role in the actual fusion process has not been experimentally demonstrated.

The HVR is located at the distal end of the C-shaped MDC domain, and points toward the M-domain catalytic site, with a distance of ~4 nm between them. It has been suggested that the C domain is an adhesion domain with potential protein–protein and protein–matrix binding surfaces. However, most of the studies that implicate this region in heterologous interactions have not identified specific regions of the C domain that are involved, and the molecular mechanism of recognition is not well understood. Different ADAMs and SVMPs have distinct HVR sequences, which results in their having distinct surface features that may play a role in binding specificity. The VAP1 structure indicates that the HVR may interact with other proteins, bringing them toward the M-domain catalytic site where they can interact directly with the catalytic cleft. These observations suggest that the HVR of both ADAMs and SVMPs could be an exosite for the cleavage of certain cell-surface molecules; that is, it may directly interact with target molecules or their associated proteins that are processed by the catalytic site. The D domain is located opposite and apart from the catalytic site, and thus, might function primarily as a scaffold that positions the catalytic site and the exosite in the proper position and orientation.

Comparison to the related structures

ADAM 10 and ADAMTS-1 C_h domains

ADAM10 and ADAM17 show less sequence similarity, particularly in the C domain, to the other canonical

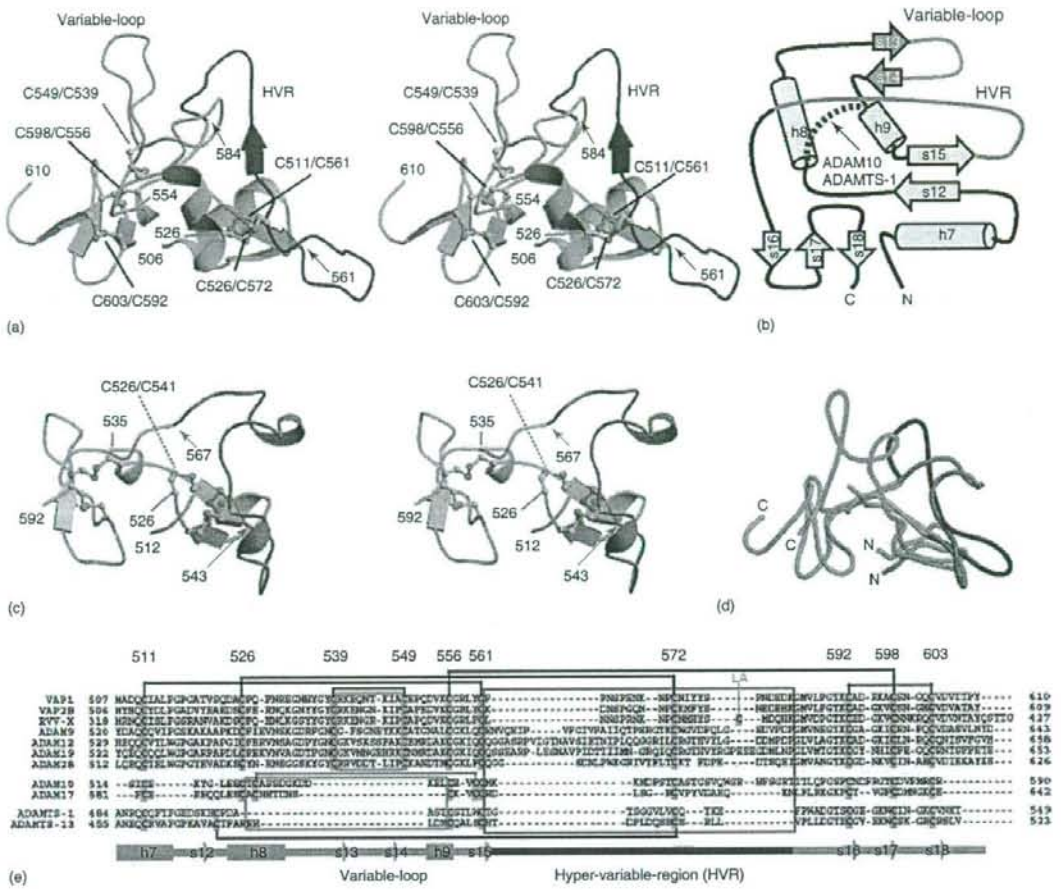

Figure 8 Structures of the hand segment (C_h segment) of VAP1 and human ADAM10. (a) Ribbon diagram of the VAP1 C_h segment in stereo. The HVR is shown in blue. The common scaffold of VAP1, ADAM10, and ADAMTS-1 is shown in cyan, and the segment lacking in ADAM10 is shown in light green. Disulfide bridges are indicated; (b) topology diagram of the C_h segment of VAP1; (c) ribbon representation of the C_h segment of ADAM10 in stereo. The HVR is shown in red. The numbering of the amino acids of ADAM10 (bovine) were changed to that of human; (d) superimposition of the C_h segments of VAP1 and ADAM10. The colors are as described for (a) and (c); and (e) structure-based alignment of the C_h segments of SVMPs, human ADAMs, and human ADAMTSs. Secondary structures of VAP1 and the disulfide bridges are represented schematically.

ADAMs. A comparison of the bovine ADAM10 DC domain structure ($ADAM10_{D+C}$)[73] and that of VAP1 reveals that these two proteins share a continuous D_s/C_w structure and C_h segment scaffold[49] (Figure 8(a–c)). The crystal structure of the MD domains of the human ADAMTS-1 has recently been determined, and it shows that the previously named disintegrin-like domain of ADAMTS-1 appears to be very similar in structure to the C_h segment of VAP1 (rmsd of 1.1 Å for 52 Cα atom positions), despite low sequence identity (~16%) between the two molecules.[23] The locations of the four disulfide bonds within the C_h segment are conserved among VAP1, ADAM10, and ADAMTS-1, which enabled us to align the three sequences. Figure 8(e) shows the sequence alignment of a selected subset of human ADAMs, ADAMTSs, and SVMPs. ADAM10 and ADAMTS-1 lack helix h8 and the variable loop that protrudes from VAP1, and have different HVR structures (the amino-terminal region of the HVR of ADAMTS-1 is disordered and has not been included in the model[23]). ADAMTSs lack the entire $D_s/D_a/C_w$ segments and their C_h segment is connected to the M domain by a connector loop (22 residues in ADAMTS-1) that wraps around the back of the M domain, resulting in a drastically different position of the C_h segment relative to the M domain compared to VAP1. ADAM10 also has a different spatial arrangement of the M and C_h